Yttrium speciation variability in bauxite residues of various origins, ages and storage conditions

Julien Couturier, Pierre Tamba Oularé, Blanche Collin, Claire Lallemand, Isabelle Kieffer, Julien Longerey, Perrine Chaurand, Jérôme Rose, Daniel Borschneck, Bernard Angeletti, et al.

▶ **To cite this version:**

Julien Couturier, Pierre Tamba Oularé, Blanche Collin, Claire Lallemand, Isabelle Kieffer, et al.. Yttrium speciation variability in bauxite residues of various origins, ages and storage conditions. 2023. hal-04290788v1

HAL Id: hal-04290788

https://hal.science/hal-04290788v1

Preprint submitted on 17 Nov 2023 (v1), last revised 17 Nov 2023 (v3)

HAL is a multi-disciplinary open access archive for the deposit and dissemination of scientific research documents, whether they are published or not. The documents may come from teaching and research institutions in France or abroad, or from public or private research centers.

L'archive ouverte pluridisciplinaire **HAL**, est destinée au dépôt et à la diffusion de documents scientifiques de niveau recherche, publiés ou non, émanant des établissements d'enseignement et de recherche français ou étrangers, des laboratoires publics ou privés.

Yttrium speciation variability in bauxite residues of various origins, ages and storage conditions

Julien COUTURIER[1*], *Pierre Tamba Oularé*[1,2], *Blanche Collin*[1], *Claire Lallemand*[1], *Isabelle Kieffer*[3], *Julien Longerey*[1], *Perrine Chaurand*[1], *Jérôme Rose*[1], *Daniel Borschneck*[1], *Bernard Angeletti*[1], *Stéven Criquet*[4], *Renaud Podor*[5], *Hamed Pourkhorsandi*[6], *Guilhem Arrachart*[5], *Clément Levard*[1**]

[1]*Aix-Marseille Univ, CNRS, IRD, INRAE, CEREGE, 13545 Aix-en-Provence, France*

[2] ISMGB, BP 84 Boké, République de Guinée

[3] OSUG, Université Grenoble-Alpes, CNRS, Grenoble, France

[4] Aix-Marseille Univ, Avignon Université, CNRS, IRD, IMBE, Marseille, France

[5] ICSM, Univ Montpellier, CEA, CNRS, ENSCM, Marcoule, France

[6] Laboratoire G-Time, Université Libre de Bruxelles, CP 160/02, 50, Av. F.D. Roosevelt, 1050, Brussels, Belgium

*couturier@cerege.fr

**levard@cerege.fr

Abstract

Bauxite residues (BRs) are highly alkaline wastes generated during alumina production from bauxite ore. Billions of tons have been accumulating worldwide for more than 100 years, they are stored in various forms, and pose environmental and societal issues. At the same time, BRs are promising secondary sources for the production of critical metals including rare earth elements (REEs). However, knowledge on REE speciation is lacking, and is consequently an obstacle to the development of large-scale extraction process.

This study analyses the influence of origin of the bauxite ore (lateritic or karstic), the storage conditions and storage time on the properties of ten BR samples, with a particular focus on the speciation of yttrium, which is used as a proxy to identify the behaviour of heavy REE.

A multi-scale approach linked yttrium speciation and the origin of the bauxite ore whereas no major variation was observed as a function of storage conditions or ageing of the BRs. Yttrium is mainly found in the form of xenotime phosphate particles in BRs of lateritic origin, while in karstic BRs, the majority of yttrium is probably adsorbed or incorporated into other minerals including iron oxyhydroxide and hydroxyapatite minerals.

1. Introduction

The global demand for metals is constantly increasing, both in terms of quantity and diversity (OECD, 2019; Zepf et al., 2014). This increase is linked to the growth of the world's population and also to the emergence of new societal needs, which consume large quantities of these resources. This is particularly true for sectors such as defense and the digital and environmental transition which makes some metals with specific physico-chemical properties highly strategic (European Commission, 2020; International Energy Agency, 2021) or even "critical" for a number of non-producing countries (British Geological Survey, 2015; Grohol & Veeh, 2023; Hatayama & Tahara, 2014; U.S. Geological Survey, 2022).

Rare earth elements (REEs), considered as one of the most critical elements according to European and American agencies (Grohol & Veeh, 2023; U.S. Geological Survey, 2022), are the focus of particular attention. The REE group includes metals from the lanthanide family (Z = 57 - 71), as well as yttrium (Y, Z = 39) and scandium (Sc, Z = 21) due to their similar physico-chemical properties. REEs are usually subdivided into two subgroups, light rare earth elements (LREEs), comprising lanthanides from lanthanum (La, Z = 57) to europium (Eu, Z = 63) and heavy rare earth elements (HREEs), including Y and lanthanides from gadolinium (Gd, Z = 64) to lutetium (Lu, Z = 71). This arbitrary distinction has no scientific basis because there is no clear physico-chemical separation between these groups, rather a progressive change in properties and behaviours, including in ionic radii (Gschneidner, 1990). Their particular electronic configuration gives them specific electromagnetic properties, making them essential for many applications in electronics, manufacturing, medicine, and renewable energy, among others (Balaram, 2019). China controls almost the entire REE value chain (Gauß Roland et al., 2021), making the supply of REEs worldwide extremely vulnerable, as revealed in 2010, when China's quota policy causes a "REE crisis" in Europe and the US (Chen & Zheng, 2019).

Beyond these economic and geopolitical considerations, primary extraction also poses often neglected environmental and social problems (Eheliyagoda et al., 2020), due to the huge quantities of energy required and of waste generated (Adewuyi et al., 2020; Farjana et al., 2019), as well as social conflicts and accidents (Goodland, 2012; Scheidel et al., 2020). All these impacts are further amplified by the general decline in ore grades (Prior et al., 2012).

Faced with the ever-increasing demand for critical metals, the depletion of resources and the environmental and social crises associated with their extraction, a paradigm shift is urgently needed for the sustainable production of these metals. In particular, in the context of circular economy, there is a need to develop processes for extracting metals from secondary sources.

Since 2010 and the "REE crisis", the search for secondary sources of REEs has become a hot research topic with almost 350 papers published in 2022 whereas before 2010, fewer than 10 papers were published on this topic per year (**Figure *1*** A). This vast literature can be divided into two main

categories. First, papers related to concentrated wastes (i.e. that contain REE concentrations above 1 wt%), which consist mainly in end-of-life products or product manufacturing scraps, and account for the majority of publications. In this category, permanent magnets are the most widely studied followed by waste from electrical and electronic equipment (WEEE), batteries, phosphors, catalysts or polishing powders (Belfqueh et al., 2022; Ramprasad et al., 2022; Yang et al., 2013). Second, diluted wastes (i.e. that contain REE concentration below 1 wt%) are usually more complex matrices (Binnemans et al., 2015) that are potentially more difficult to exploit given the low concentrations of REEs but which also attract considerable attention. This category includes mining and industrial wastes such as bauxite residues (BRs), phosphogypsum, coal fly ash, acid mine drainage, mine tailings or wastewater (Binnemans et al., 2015; Dupont & Binnemans, 2015; Hermassi et al., 2022; Peiravi et al., 2021). In this category, BRs are one of the most frequently cited and studied as a potential source for REEs (20-35% of identified papers in the last five years).

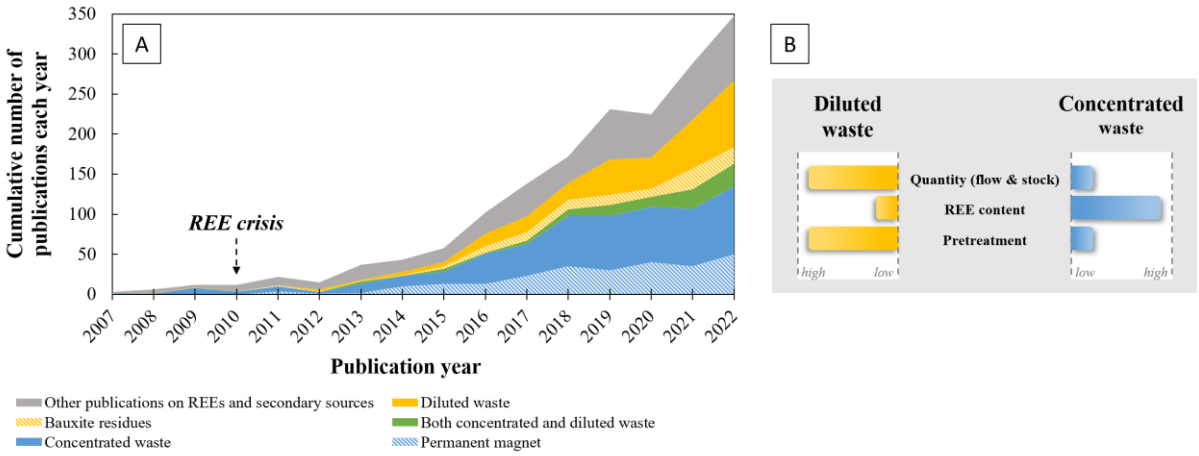

Figure 1: *(A) Evolution of cumulative number of scientific papers containing "rare earth elements" and "secondary sources" keywords, from 2007 and 2022, separated into several categories (source Web of Science). The "Concentrated waste" category contains the keywords: "magnet", "WEEE", "phosphor", "battery", "catalyst", "polishing waste". The "Diluted waste" category contains the keywords: "Bauxite residues", "phosphogypsum", "coal fly ash", "mine drainage", "mine tailings", "wastewater". (B) Conceptual scheme of the difference in properties in diluted and concentrated waste.*

Bauxite residues (BRs), also known as "red mud" when hydrated, are wastes generated during the production of alumina using the Bayer process. During this process, the primary bauxite ore, rich in aluminium (Al), is digested with concentrated soda under pressure, leaving a highly alkaline and sodic residue at the end of the process. BRs are mainly composed of iron oxide but also contain a cocktail of toxic and critical metals (Borra et al., 2016; Smith, 2009). REEs, which are naturally present in bauxite ore, are concentrated in BRs as a result of the Bayer process and can reach more than 2500 mg/kg (2500 ppm) (Qu & Lian, 2013; Rayzman, 1998; Wagh & Pinnock, 1987), which makes BRs a potentially good secondary source (Deady et al., 2014) with many advantages over concentrated waste (**Figure *1*** B). First, BRs represent a huge potential reserve of REEs: for every ton of alumina produced, between

1 and 2 tons of BRs are generated (Borra et al., 2016). Today, it is estimated that approximately 170 Mt of BRs are generated each year, i.e. producing a global stockpile exceeding 4 billion tons (Evans, 2016; International Aluminium Institute, 2023). These stocks are generally easily accessible, as they are located in storage sites close to alumina plants. Moreover, with their very fine granulometry (Gräfe et al., 2011), BRs require little grinding pre-treatment, which is often described as the most energy-consuming stage of the primary extraction processes (Adewuyi et al., 2020).

However, although this residue appears to be an interesting alternative for the production of REEs, the variability of the physico-chemical properties of these residues is an obstacle to the development of a universal process of REE extraction. Several parameters may cause physico-chemical variations in the stocks of BRs available worldwide. First, essentially two types of bauxite ores are used as inputs in the Bayer process: lateritic bauxites, which account for 90% of the mineable reserves, and karstic (or karst) bauxites (Freyssinet et al., 2005). Both derive from similar processes of alteration and sedimentation (weathering, transportation and deposition), leading to the formation of an Al-rich ore. The difference lies in their bedrock lithology: lateritic bauxite deposits overlie aluminosilicate rocks while karstic deposits overlie carbonate rocks (Bardossy, 1982). Second, differences in the efficiency of the Bayer process due to different Al mineralogy depending on the type or quality of the bauxite ore and variability in the implementation of the Bayer process, may result in variable amounts of Al remaining in the mine tailings. The conditions and time of storage of the residues may also affect their physico-chemical properties. When not directly discharged into the seas and oceans, BRs are stored in different ways ranging from dry storage in the open air to storage in the form of sludge in retention ponds (Evans, 2016; Fourrier, 2020; Power et al., 2011). Aging of BRs can also induce physico-chemical variability since some residue deposits may be more than 100 years old: the Bayer process was invented at the end of the 19th century (Borra et al., 2016). Consequently, treatment or remediation attempts (cover layers, organic or inorganic amendment, etc.) have been undertaken at many sites sometimes leading to revegetation of the site despite particularly hostile conditions for life (Di Carlo et al., 2019).

This variability also results in marked differences in chemical composition and mineralogy as reported in the literature (Borra et al., 2016; Evans, 2016; Ma et al., 2022; Xue et al., 2016). Although the chemical and mineralogical variability is fairly well documented for major elements such as Fe and Al, very little information is available on REE speciation (i.e., the chemical environment) in BRs. Also, most studies that do address REE speciation are based on a microscopic approach (using electron probe microanalyses (EPMA) or scanning electron microscopy coupled with energy dispersive X-ray spectrometry (SEM/EDS)) and rely on elemental co-localization to identify REE bearing phases, which are based on assumptions, rather than on direct speciation analyses (Gentzmann et al., 2021; Ochsenkiihn-Petropulu et al., 1996; Rivera et al., 2019; Vind et al., 2018). In addition, existing studies rarely investigate the influence of origin of the bauxite ore, or the time and conditions of storage of BRs. Indeed, detecting low concentration phases and elements in such complex matrices is far from easy, plus detailed characterisation of REEs in BRs requires state of the art facilities such as synchrotron sources.

In the present study, the physico-chemical properties, chemical composition, mineralogy and yttrium speciation of ten BR samples with different origins, ages and storage conditions were characterised. Yttrium was used as a proxy for HREEs thanks to its similar physico-chemical behaviour (Borst et al., 2020; Lallemand et al., 2022; Pingitore et al., 2014). Improving knowledge of the REE speciation in BRs and the factors that influence it will pave the way for the development of extraction processes that account for the specificity of the targeted BRs in terms of origin, storage conditions and time (Deady et al., 2014). Such perspectives are discussed in light of our results.

2. Materials and methods

2.1. Materials and sampling

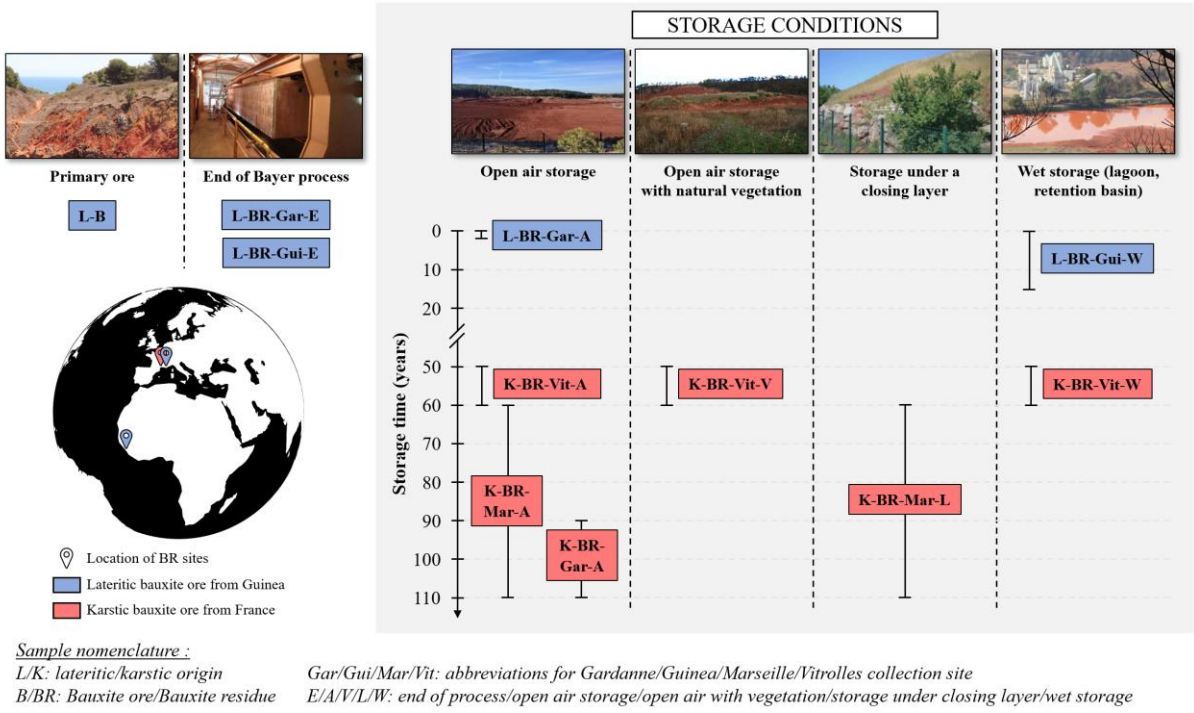

Figure 2: *Presentation of the study samples according to the origin of the ore, age, storage conditions and associated nomenclature*

The sample bauxite residues were categorized in two types: those generated from a lateritic-type bauxite ore located in Guinea (Boké region), and those generated from a karstic-type bauxite ore located in the south of France (Provence region), hereafter referred to respectively as "lateritic BRs" and "karstic BRs" for the sake of simplicity. These ten residues were collected from four different tailing sites: three in France (Gardanne "Gar", Vitrolles "Vit", Marseille "Mar") and one site in Guinea "Gui" (Fria plant site) from three alumina production plants which use the Bayer process. Samples were collected at several places: (i) directly at the end of the alumina extraction process (E suffix), after the filter press (L-BR-Gar-E) or the last scrubber (L-BR-Gui-E), (ii) from open-air storage sites (A suffix) at the surface (maximum 30 cm depth) of the deposits (L-BR-Gar-A, K-BR-Vit-A, K-BR-Mar-A, K-BR-Gar-A), one of which in a heavily vegetated area (suffix V) (K-BR-Vit-V), (iii) from a storage site under a vegetated capping layer (suffix L), at a depth of 1 m below the surface (K-BR-Mar-L) and (iv) from wet storage sites (suffix W) as lagoon or retention basin (L-BR-Gui-W, K-BR-Vit-W). The storage conditions and aging times (from 0 to 100 years) of the residues are detailed in ***Table 1*** and **Figure *2***.

The initial lateritic bauxite ore (L-B) sample was supplied by Alteo company, a producer of alumina at the Gardanne site which, at that time, used lateritic bauxite ores imported from Guinea. No bauxite ore of karstic origin representative of the studied karstic BR samples was used in the present study because

189 either the plant concerned had closed down or the supply had been switched to lateritic bauxite ores, as
190 was the case in Gardanne between the 1970s and 1990s (Arnaud & Guillon, 1989).
191 Before the experiments began, all the samples were dried at between 60-70 °C then manually ground to
192 < 125 µm using an agate mortar and homogenized. The resulting dry materials were stored at ambient
193 pressure and temperature.

Table 1: *Detailed description of the samples cited in this article*

Name of sample	Type of sample	Origin of bauxite	Plant	Sampling location	Storage conditions	Some known detailed conditions	Storage time
L-B	Bauxite ore	Lateritic (Guinea)	/	*	/	/	/
L-BR-Gui-E	Bauxite residue	Lateritic (Guinea)	Fria plant (Guinea)	At the plant (end of process)	End of Bayer process (after the last scrubber)	/	/
L-BR-Gui-W	Bauxite residue	Lateritic (Guinea)	Fria plant (Guinea)	Dote dam, Guinea	Wet storage (Tropical climate)	/	~0-15 years***
L-BR-Gar-E	Bauxite residue	Lateritic (Guinea)	Gardanne plant (France)	At the plant (end of process)	End of Bayer process (after the filter press)	/	/
L-BR-Gar-A	Bauxite residue	Lateritic (Guinea)	Gardanne plant (France)	Gardanne tailing site (Mange-Garri)	Storage in the open air (Mediterranean climate)	Occasional watering / BR was mixed with compost at this location	~1 year
K-BR-Gar-A	Bauxite residue	Karstic (France)	Gardanne plant (France)	Gardanne tailing site (Mange-Garri)	Storage in the open air (Mediterranean climate)	Occasional watering / soil amendment in the 1960's / light vegetation cover	~**90**-110 years**
K-BR-Mar-A	Bauxite residue	Karstic (France)	Saint-Louis-les-Aygalades plant (France)	Marseille tailing site (La Delorme)	Storage in the open air (Mediterranean climate)	/	~**60**-110 years**
K-BR-Mar-L	Bauxite residue	Karstic (France)	Saint-Louis-les-Aygalades plant (France)	Marseille tailing site (La Delorme)	Storage under closing layer (Mediterranean climate)	Backfill layer and vegetation (capping layer)	~**60**-110 years**
K-BR-Vit-A	Bauxite residue	Karstic (France)	Saint-Louis-les-Aygalades plant (France)	Vitrolles tailing site (Griffon)	Storage in the open air (Mediterranean climate)	Presumed landfill (sewage sludge spreading)	~**50**-60 years**
K-BR-Vit-V	Bauxite residue	Karstic (France)	Saint-Louis-les-Aygalades plant (France)	Vitrolles tailing site (Griffon)	Storage in a heavily vegetated area (Mediterranean climate)	Vegetation cover / backfills presence / presumed landfill	~**50**-60 years**
K-BR-Vit-W	Bauxite residue	Karstic (France)	Saint-Louis-les-Aygalades plant (France)	Vitrolles tailing site (Griffon)	Wet storage, in a retention basin (Mediterranean climate)	Presumed landfill and backfills presence	~**50**-60 years**

** Supplied by Alteo, the company that currently manages the Gardanne plant.*
*** Uncertainty concerning the time of use of the storage site. Dry samples collected on the surface and therefore considered to be young (in **bold** in the table).*
**** Difficult to determine the exact age of storage of liquid samples in the dam because of potential transfer between young and old residues. Liquid samples collected on the surface can be considered to be relatively young (0-15 years) compared to the age of the dam (40 years).*

2.2. Characterisation of the samples

2.2.1. pH and conductivity

For pH and electrical conductivity measurements, aqueous suspensions with a 1/5 solid/liquid ratio (1 g of material in 5 mL of distilled water) were prepared according to ISO 10390:2021. Measurements were made at 20 °C with two replicates after 2 h of stirring and 24 h of decantation.

2.2.2. Chemical composition

Preparation and bulk chemical analyses were conducted at CEREGE (France). The samples were digested by alkaline fusion using 100 mg of sample mixed with 500 mg of previously dried flux (49.5% lithium tetraborate, 49.5% lithium metaborate, 1% LiBr) and placed in an oven (Malvern Panalytical Claisse LeNeo) to undergo specific high refractory material digestion (up to 1050 °C for 22 min). The resulting fusion pearl was immediately dissolved in 40 mL of nitric acid (3-4 wt%). After appropriate dilution in distilled water, trace elements (<1000 µg/L) were analysed by inductively coupled plasma mass spectrometry (ICP-MS, Perkin Elmer 300X quadrupole) and major elements (>1000 µg/L) were analysed by inductively coupled plasma optical emission spectroscopy (ICP−OES Perkin Elmer Optima 4300 DV).

Three replicates were made of each analysis, and the results (concentration in mg/kg dry weight) are expressed along with the average and the standard deviation of the three samples.

2.2.3. Mineralogy

Mineralogy was performed by X-ray diffraction (XRD) at 40 kV and 40 mA on a PANalytical X'Pert Pro (Malvern Panalytical, UK) diffractometer equipped with a rear monochromator and a cobalt anticathode (λ = 1.79 Å) at CEREGE (France). Powder samples were deposited on low background silicon plates with a drop of ethanol and scanned from 5 to 75° (2θ) with a step size of 0.033° and a total counting time of 3 h. The sample was rotated at 15 rpm during analysis to improve the statistics. Phase identification was performed using the X'pert Highscore plus software (Malvern Panalytical) with the PDF-2 ICDD (International Center for Diffraction data, Powder Diffraction Files 2) and COD (Crystallography Open Database).

2.2.4. Microscale observations

Microscale observations were performed using a Quattro S Environmental Scanning Electron Microscope (ThermoFisher) coupled with a XFlash6 / 100 Energy Dispersive X-ray Spectrometer with Quantax 400 software (Bruker) (SEM/EDS) (ICSM, France). The L-BR-Gui-E and K-BR-Mar-A powder samples were embedded in resin (Araldite 2020) and then polished (using silicon carbide and diamond) with oil. The cross-sections were then coated with carbon, and copper tape was used to ensure good conduction during microscopy. Series of elemental distribution maps (12×12 and 15×15, ×500 magnification) were first recorded (30 kV, 200 kcps, 20 min for each) to locate particles or grains containing Y over a large area (6-8 mm²). Once the particles were identified, EDS point analyses (15

kV, 100 kcps, 1 min), as well as EDS elemental maps of the selected areas (12 kV, 50 kcps, 20 min) were performed. Finally, quantitative-EDS elemental maps were performed to avoid interference between elements. These maps were produced by integrating 8×8 pixels from the qualitative EDS maps to increase the counting statistics and reduce calculation time.

2.2.5. Yttrium speciation by X-ray absorption spectroscopy (XAS)

XAS spectra at Y K-edge (17.038 keV) were recorded at the European Synchrotron Radiation Facility (ESRF, Grenoble, France) on beamline BM30 (CRG-FAME beamline) (Chaurand et al., 2025).

Incoming photon flux energy was modulated using a Si(220) double crystal monochromator and higher harmonics were suppressed using Rh-curved mirrors. The data were collected in the step-by-step mode with a beam size of 200×150 µm.

Samples of bauxite ore and BRs were prepared as pure pellets (~30 mg), and model compounds were prepared as pellets diluted with polyvinylpyrrolidone (PVP). For the latter, the dilution ratio with PVP was calculated to obtain an optimal $\Delta\mu_{theoritical}$ of 1 with ABSORBIX software (v3.02) (Michalowicz et al., 2009).

During the experiment, incoming X-ray beam energy was calibrated and regularly checked using a reference metal foil of Y. Each sample was measured in an He cryostat at 10-20 K to prevent beam damage. Spectra were obtained in fluorescence mode for bauxite ore and BR samples (average of 3 to 9 scans depending on the signal to noise ratio), and in transmission mode for model compounds (1 to 3 scans), except for the Y-doped hematite model compound which was run in fluorescence mode due to the relatively low concentration of Y. XAS spectra (XANES and EXAFS) were recorded from 16.85 to 17.58 keV (k = 12 A^{-1}) with an energy step of 5 eV between 16.85 and 17 keV (1s counting time), of 0.5eV from 17 to 17.085 keV and a k step of 0.05 A^{-1} from 17.085 to 17.58 keV. Calibration, merging and normalization were performed with XAS-Viewer software (Larch, v0.9.65) (Newville, 2013).

A library of Y reference compound spectra was used to identify Y species in bauxite ore and BRs (Couturier et al., 2022). The library consisted of commercial references (purity >99.9%): yttrium oxide (Y_2O_3; Acros Organics), yttrium carbonate ($Y_2(CO_3)_3 \cdot xH_2O$; Alfa Aesar), yttrium phosphate ($YPO_4 \cdot xH_2O$ Alfa Aesar) hereafter "medium crystalized xenotime YPO_4" or "mcxYPO_4", but also synthesized references (see protocols and XRD in SI): yttrium hydroxide ($Y(OH)_3$), yttrium phosphate (YPO_4) with different phase and crystallinity (churchite, low and high crystallized xenotime), Y-adsorbed on montmorillonite ($(Na,Ca)_{0,3}(Al,Mg)_2Si_4O_{10}(OH)_2 \cdot xH_2O$), Y-doped Calcite ($CaCO_3$), Y-doped hematite ($Fe_2O_3$), low and high crystallized Y-doped hydroxyapatite ($Ca_5(PO_4)_3(OH)$).

Linear combination fitting (LCF) of the XANES region was performed from 17000 to 17220 eV with a maximum of three components (adding a fourth component did not improve fits) using XAS Viewer software (Larch, v0.9.65) (Newville, 2013). The reduced-chi-square value (χ^2_{red}), which accounts for degrees of freedom in the fit, was used to compare the relative quality of two fits that use the same

interval but a potentially different number of variables. A change between two fits is considered statistically significant when the ratio of their two reduced-chi-square is greater than two standard deviations, according to the reference (Kelly et al., 2008). In our case, this criterion was used to identify all fits that were significantly identical to the best fit, which were then defined as "good fits". The value of the criterion was 1.185 and was obtained with the number of points in the fitting interval (N = 237-239) and the number of variables in the fit (V = 3-4).

3. Results and discussion

3.1. pH and electrical conductivity

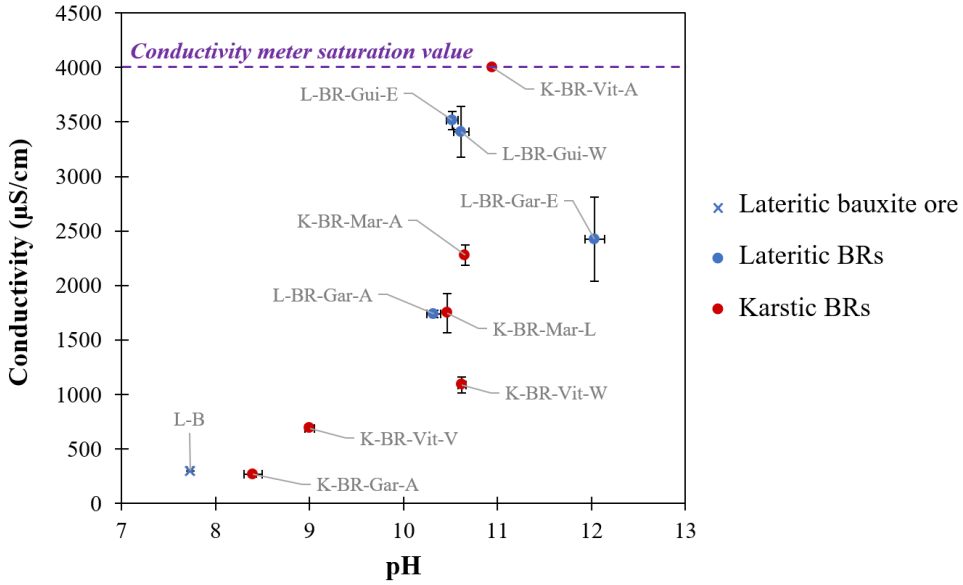

Figure 3: *Conductivity of all the samples as a function of pH (solid/liquid ratio = 1/5, 20 °C) (blue = lateritic-type, red = karstic-type).*

pH and conductivity varied widely among the samples (**Figure *3***, ***Table S1***). The bauxite ore sample (L-B) had an almost neutral pH and very low conductivity (<300 µS/cm), whereas the BRs had alkaline pH ranging from 8.4 to 12, and strongly varying conductivity, i.e. from 266 µS/cm to >4 mS/cm (saturation value). The high variability observed is nevertheless consistent with that reported in the literature (Gräfe et al., 2011; Snars & Gilkes, 2009).

The alkaline nature and high conductivity of BRs are due to the contact between bauxite ore and concentrated soda during the Bayer process. In addition to solubilizing Al, excess OH^- and Na^+ ions in the residue are responsible for the high pH and conductivity (Di Carlo et al., 2019; Gräfe et al., 2011). Many parameters can influence both pH and conductivity of the BRs. During the Bayer process, the concentration of the NaOH solution, the quality of the washing steps or the inclusion of a filtration step determine the alkalinity and salinity of the BR at the outlet of the plant, among other things (Power et al., 2011). During storage, locally strong increases in pH and conductivity can occur at the surface of the deposit, resulting in the formation of efflorescence (Di Carlo et al., 2019; Wu et al., 2020), mainly in the form of a thin white layer composed of Na_2CO_3 and $NaHCO_3$. This phenomenon has already been observed at the Vitrolles site (Fourrier, 2020) and may explain the high conductivity of K-BR-Vit-A. However, a decrease in pH and conductivity is most often observed as a function of the storage time of the deposit. The decrease is related to the leaching of alkaline soluble compounds by natural weathering (mainly rainfall), to the slow carbonation of BRs by atmospheric CO_2 or even to the activity of microorganisms and plants (Cusack et al., 2019; Di Carlo et al., 2019; Khaitan et al., 2010; Kong, Guo,

et al., 2017; Macías-Pérez et al., 2022; Zhu et al., 2016). This aging effect was particularly visible in the oldest sample, K-BR-Gar-A. Organic, inorganic, acidic or seawater amendments also lead to the neutralization of BRs, which is one of the most desired effects when the aim is remediation or use of these wastes around the world (Fourrier et al., 2021; Jones et al., 2012; Khaitan et al., 2009, 2010; Klauber et al., 2011; Kong, Li, et al., 2017; Menzies & Kopittke, 2021; Wong & Ho, 1991). Neutralization of BRs is the main factor that enables the natural establishment of micro-organisms and vegetation (Di Carlo et al., 2019; Santini & Fey, 2013; Xue et al., 2016), as can be seen at the K-BR-Gar-A and L-BR-Vit-V sites.

The age or storage conditions of the BRs thus appear to have an influence on their pH and conductivity, but many other parameters also come into play, making it difficult to make clear correlation, especially when the history of operations at the site is difficult to trace.

3.2. Chemical composition

Table 2: *Chemical composition by mass of major elements (Fe, Al, Ti, Si, Ca), Y and sum of all REEs (including Y and Sc) present in our samples, obtained by ICP-MS and ICP-OES after alkaline fusion (3 replicates).*

Sample	Fe (wt%)	Al (wt %)	Ti (wt %)	Si (wt %)	Na (wt %)	Ca (wt %)	Y (mg/kg)	ΣREEs (mg/kg)
L-B	14.51 ± 0.08	23.11 ± 0.04	1.57 ± 0.01	1.00 ± 0.01	0.01 ± 0.02	0.00 ± 0.01	34 ± 2	218 ± 6
L-BR-Gui-E	31.24 ± 0.11	8.05 ± 0.14	3.26 ± 0.08	2.02*	1.94 ± 0.03	1.16 ± 0.09	102 ± 2	562 ± 15
L-BR-Gui-W	32.33 ± 1.34	8.73 ± 0.35	3.40 ± 0.18	2.31*	1.98 ± 0.12	1.46 ± 0.11	101 ± 6	563 ± 25
L-BR-Gar-E	31.48 ± 0.45	5.56 ± 0.11	4.74 ± 0.10	1.97 ± 0.02	2.23 ± 0.09	4.28 ± 0.09	118 ± 0	727 ± 4
L-BR-Gar-A	31.90 ± 0.23	6.49 ± 0.03	5.15 ± 0.04	1.92 ± 0.02	2.54 ± 0.04	2.82 ± 0.04	123 ± 2	778 ± 13
K-BR-Gar-A	28.47 ± 0.65	8.97 ± 0.06	2.37 ± 0.03	3.13 ± 0.06	1.28 ± 0.04	3.53 ± 0.05	226 ± 4	1792 ± 24
K-BR-Mar-A	29.43 ± 1.01	5.60 ± 0.17	4.08 ± 0.14	3.20 ± 0.11	3.06 ± 0.15	4.45 ± 0.02	226 ± 8	2261 ± 74
K-BR-Mar-L	39.02 ± 0.13	6.22 ± 0.03	4.52 ± 0.02	2.76 ± 0.01	2.34 ± 0.02	0.85 ± 0.01	265 ± 10	2702 ± 128
K-BR-Vit-A	25.31 ± 0.51	9.92 ± 0.15	2.70 ± 0.04	3.67 ± 0.07	5.91 ± 0.27	1.85 ± 0.04	219 ± 2	1924 ± 18
K-BR-Vit-V	21.64 ± 0.28	7.96 ± 0.05	2.47 ± 0.02	5.25 ± 0.03	3.04 ± 0.06	5.01 ± 0.04	184 ± 1	1549 ± 11
K-BR-Vit-W	20.80 ± 0.06	7.78 ± 0.03	2.47 ± 0.01	5.88 ± 0.02	3.79 ± 0.22	6.01 ± 0.02	199 ± 3	1668 ± 7

** Silicon was only measured in one replicate of L-BR-Gui-E and L-BR-Gui-W samples.*

The chemical composition of the samples is listed in ***Table 2*** (additional elements are reported in ***Table S2***). The bauxite ore sample (L-B) mainly contained aluminium (Al, 23.1 wt%) and iron (Fe, 14.5 wt%) while BR samples mainly contained Fe (20-39 wt%), Al (5-10%), silicon (Si, 2-6 wt%) and titanium (Ti, 2-5 wt%). The main difference in composition between bauxite ore and the BR samples was due to Al extraction during the Bayer process. The Bayer process was also at the origin of the non-negligible sodium content (Na, 1.3-5.9 wt%) and calcium content (Ca, 0.8-6.0 wt%) in the BRs, whereas these elements were not present in the L-B sample. The presence of Na is due to digestion of bauxite ore with caustic soda (NaOH) and the presence of Ca to the addition of lime (CaO, $Ca(OH)_2$) during preliminary desilication and causticization (Borra et al., 2016; Smith, 2009).

Among the minor elements, the amount of total REEs (including Y and Sc) in the L-B sample was 218 mg/kg while total REE contents in BRs ranged from 562 to 2702 mg/kg. The enrichment of the REE content in BRs is specific to the Bayer process, as these elements are not released by soda during the process and are consequently concentrated in the residues. Individually, REE concentrations agree with their natural occurrence, ranked in decreasing order: Ce, followed by Y, La, Nd and Sc and the other REEs (***Table S2***).

Despite the significant differences between the BR samples considered in the present study, in terms of their ore origin, storage conditions, ages, as well as pH and conductivities, variations in the concentrations of the major elements remain limited compared to the variety of compositions reported in the literature (Binnemans et al., 2015; Evans, 2016; Gräfe et al., 2011; Khairul et al., 2019; Snars &

Gilkes, 2009; Xue et al., 2016). In particular, no correlation was found between the variations in the concentration of these elements and their storage time, thereby confirming some findings reported in the literature (Cusack et al., 2019). However, some slight variations in the composition of BRs can be explained by the history of activities at the storage site concerned or during the implementation of the Bayer process. To give an example, aerial image archives have proven the presence of construction site landfills in the lower part of the Vitrolles tailing site over the last 30 years, which correspond to the areas where the K-BR-Vit-V and K-BR-Vit-W were sampled (Fourrier, 2020). The addition of Si and Ca rich materials is probably responsible for lower concentrations of Fe, Al and Ti and higher concentrations of Si and Ca compared to the K-BR-Vit-A sample, which was collected from the upper part of the same tailing site and has never been in contact with these landfills. However, the difference in Al content between L-BR-Gui-E (8.0 wt%) and L-BR-Gar-E (5.6 wt%) could also be due to differences in the quality of the ore and/or in the performance of the Bayer process.

In contrast to major elements, the origin of the bauxite ore has a strong influence on REE content in BRs (657 ± 112 mg/kg (n = 4) for lateritic BRs and 1983 ± 429 mg/kg (n = 6) for karstic BRs). Indeed, karstic bauxites are known to have higher concentrations of REEs than lateritic bauxites (Binnemans et al., 2015; Borra et al., 2016; Vind et al., 2018), and can reach 1000 mg/kg or more (Liu et al., 2016; Mondillo et al., 2019). This difference has been widely reported and is usually attributed to the "pH-barrier" of the underlying alkaline carbonate rock that tends to favour REE concentration in karstic bauxites (Gentzmann et al., 2021). Consequently, the difference is carried over to the BRs with concentrations of up to 2702 mg/kg in the K-BR-Mar-L sample, which is more than ten times the average for the earth's crust ($\sum$REEs ≈ 240 mg/kg) (Haynes, 2014). The high REE contents in BRs originating from karstic bauxite ores make them promising secondary sources of REEs for the future. In comparison, some natural deposits currently being exploited for their REEs contain less than 1 wt% REEs (Davris et al., 2017; Huang et al., 2021; M. Y. H. Li et al., 2019).

The specific karstic/lateritic signature in terms of the chemical compositions of BRs can be also observed in other elements. For example, P, Cr, V, Ga are more abundant in lateritic BRs, while Si, Mg, Mn, Sr, Ni, Pb As, Co are present at higher concentrations in karstic BRs. Finally, among the elements present in the BRs (***Table S2***), we also noted the presence of significant quantities of Ti (up to >5 wt%), Mg (up to >3000 mg/kg in karstic BRs), Zr (up to >2000 mg/kg), P (up to >2000 mg/kg in lateritic BRs), V (up to >1500 mg/kg in lateritic BRs), Cr (up to >1500 mg/kg in lateritic BRs), Mn (up to >800 mg/kg in karstic BRs), Sr (up to >400 mg/kg in karstic BRs), Ni (up to >300 mg/kg in karstic BRs), which are also considered as critical elements by the European Commission or the USGS (Grohol & Veeh, 2023; U.S. Geological Survey, 2022), and for which the possibility to use BRs as a secondary source remains to be investigated.

3.3. Chondrite-normalized REE profiles

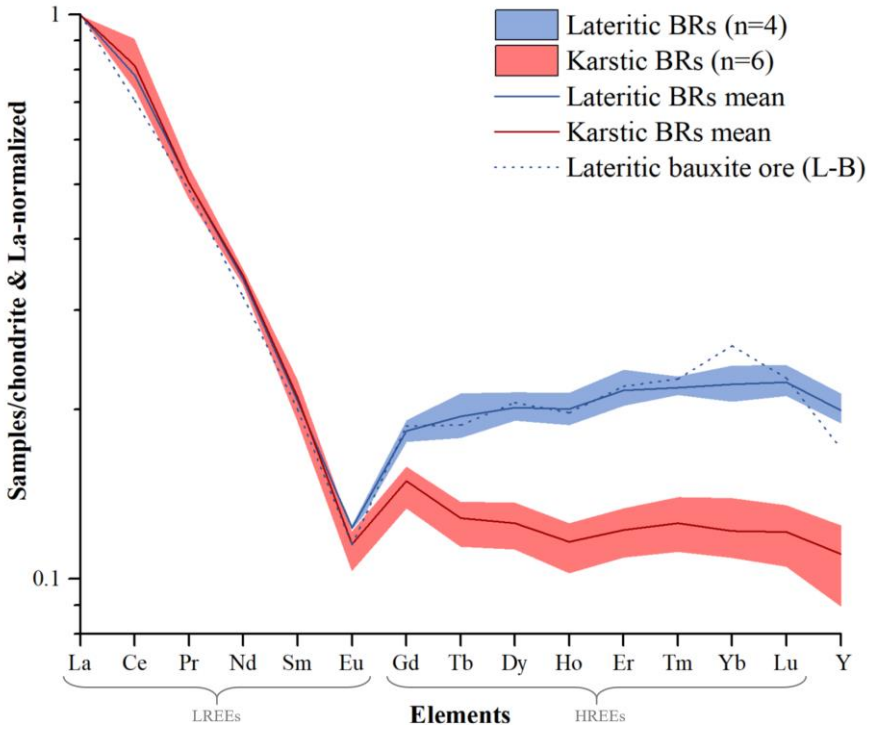

Figure 4: *Patterns of chondrite and lanthanum-normalized rare earth elements in all the bauxite residue samples studied here, separated according to the origin of the ore. The normalized spectrum of lateritic bauxite ore sample is plotted for the purpose of comparison. The normalized values come from* (Taylor & McLennan, 1985)

For a more in-depth analysis of the observed differences between lateritic and karstic BRs with respect to REEs, chondrite-normalized REE profiles are plotted by normalizing each REE content by the corresponding value in the chondrites (Taylor & McLennan, 1985), (**Figure *4***, ***Table S3***). In order to compare samples independently of their total REE content, the REE profiles are also normalized by the lanthanum value for each sample.

All the BRs showed dominance of LREEs over HREEs, which decreased with an increase in Z, as often reported for bauxites in the literature [69], [70]. The Ce and Eu anomalies, defined as the $\frac{Ce_N}{\sqrt{(La_N * Pr_N)}}$ and $\frac{Eu_N}{\sqrt{(Sm_N * Gd_N)}}$ ratios also presented similar values (1.0 to 1.3 and 0.6 to 0.7 respectively), when we compared BR compositions (***Table S4***). Interestingly, a difference appeared in the behaviour of HREEs depending on the origin of the bauxite ore. Evidence for a relative enrichment of HREEs, also visible on Y, was found in lateritic BRs compared to in karstic BRs. This variation can be characterised by the value of the slope of the REE pattern, defined as the ratio of normalized La_N/Lu_N values, which is lower for lateritic BRs (4.2 to 4.7) than for karstic BRs (7.4 to 9.5) (***Table S4***). It is also important to note that the lateritic bauxite ore sample (L-B) followed the same pattern as the lateritic BRs despite a 2 to 4 times lower REE concentration. This supports the conclusion that the differences observed in the HREEs are characteristic of the origin of the bauxite ore, as, when we compared the

REE profiles of L-B and lateritic BRs, the Bayer process had no effect on the relative proportions of the REEs.

Differences in REE patterns may be the signature of different speciation (Bea, 1996). **Figure *4*** suggests that HREEs bearing phases in BRs differ depending on the origin of the bauxite ore. This hypothesis was reinforced by further analysis of the chemical data. For example, the scatterplot between P and HREEs shows that HREEs concentration is correlated with the concentration of P in lateritic BRs, whereas no correlation was apparent in karstic BRs (***Figure S2***). To identify the HREE-bearing phases and the potential association of HREEs with P in the BRs, the mineralogy of the samples was next examined from a macroscopic and microscopic perspective, as described in the following sections.

3.4. Mineralogy

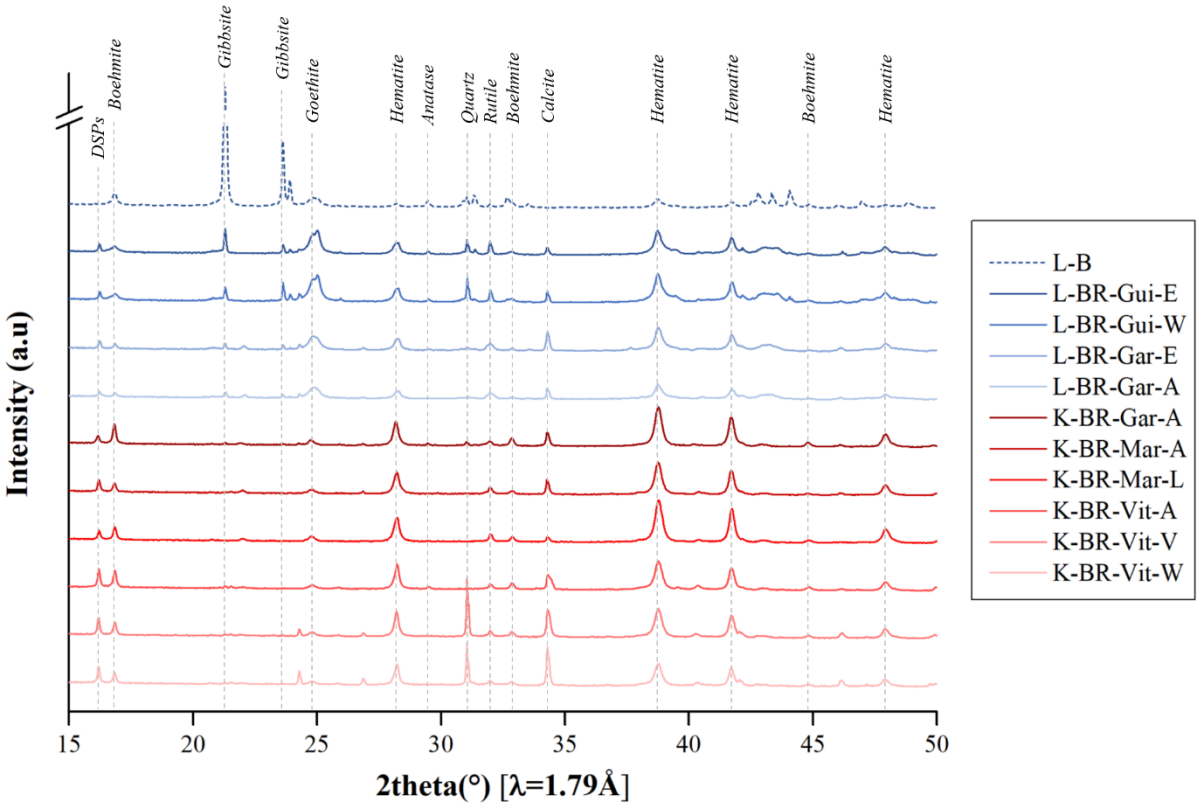

Figure 5: *X-ray diffraction patterns of the studied bauxite ore (L-B) and bauxite residue samples sorted by origin of the ore (blue = lateritic-type, red = karstic-type). Identification of the main peaks of the major phases. DSPs: desilication products*

The X-ray diffraction (XRD) patterns are reported in ***Figure 5***. In agreement with the elemental composition, the mineralogy of the lateritic bauxite ore sample (L-B) was dominated by Al phases, mostly in the form of gibbsite ($Al(OH)_3$). Gibbsite is known to be the main Al phase in lateritic bauxites characterised by weathering under a tropical climate (Baioumy, 2016; Bhukte et al., 2020; De Oliveira et al., 2016; Negrão & Costa, 2021; Sidibe & Yalcin, 2018; Vind et al., 2018), although diaspore (AlO(OH)) may be encountered in certain cases (Gu et al., 2013). Also, karstic bauxites (not studied here) often contain boehmite (AlO(OH)) as the main Al phase (Kloprogge et al., 2002; Mondillo et al., 2019; Radusinović & Papadopoulos, 2021; Reinhardt et al., 2018) even if gibbsite or diaspore phases are the main phases in some non-Mediterranean karstic bauxites (Z. Li et al., 2013; Torró et al., 2017). The effect of the Bayer process transforming bauxite ore into BR is clearly visible on XRD diffractograms. The majority of the Al phases contained in L-B were extracted showing the Fe phases to be predominant in BRs as hematite (Fe_2O_3) or goethite (FeO(OH)). The decrease in the Al phase in the BRs also brought out minor Ti phases, such as anatase or rutile (TiO_2), and Si, as quartz (SiO_2) which were masked in L-B due to the limit of detection of this technique (≈1 wt%). Similarly, calcite ($CaCO_3$) and aluminosilicate phases (cancrinite, sodalite, vishnevite) corresponding to desilication products

(Gräfe et al., 2011; Radomirovic et al., 2013; Senaputra et al., 2012) were observed in the XRD patterns of BRs. These results are consistent with data reported in the literature (Evans, 2016; Gentzmann et al., 2021; Khairul et al., 2019; Klauber et al., 2011).

The mineralogy of all the BR samples was relatively similar, except for some slight variations that mainly depended on the origin of the bauxite ore. Gibbsite (main peak at $\theta = 21.3°$) was not observed from the XRD pattern of karstic BRs. The intensity of the boehmite-related peak (main peak at $\theta = 16.9°$) was more intense in the XRD pattern of karstic BRs than in the XRD pattern of lateritic BRs, confirming reports on karstic bauxites in the literature (Kloprogge et al., 2002; Mondillo et al., 2019; Radusinović & Papadopoulos, 2021; Reinhardt et al., 2018). Iron-containing phases were present as a mixture of hematite and goethite, but relatively speaking, the intensity of hematite peaks was far greater than that of the goethite peaks in karstic BRs. The intensity of the aluminosilicate peak (main peak at $\theta = 16.2°$) was also greater in karstic BRs.

In agreement with the chemical composition, the effect of construction site backfill during storage of K-BR-Vit-V and K-BR-Vit-W is visible here due to more intense quartz ($\theta = 31.0°$) and calcite peaks ($\theta = 34.3°$) on the diffraction patterns. Similarly, we attribute the higher gibbsite and quartz peaks in L-BR-Gui-E and L-BR-Gui-W, compared to the other lateritic BRs on the diffractograms, to the quality of the ore or to the performance of the Bayer process. Indeed, the bauxite ore used at Fria plant is reputed to be of lower quality than that used at the Gardanne plant, due to its higher silica content, which hampers aluminium extraction.

The structural analysis performed by XRD revealed differences in the mineralogy of the major phases of BRs depending on the origin of the bauxite ore, but no other drastic mineralogical variation were found related to the age or storage conditions of the BRs. However, other characterisation techniques are needed to investigate the possible REE phase differences mentioned earlier in more detail3.3.

3.5. Microscopic and macroscopic evidence of speciation

3.5.1.SEM/EDS observations

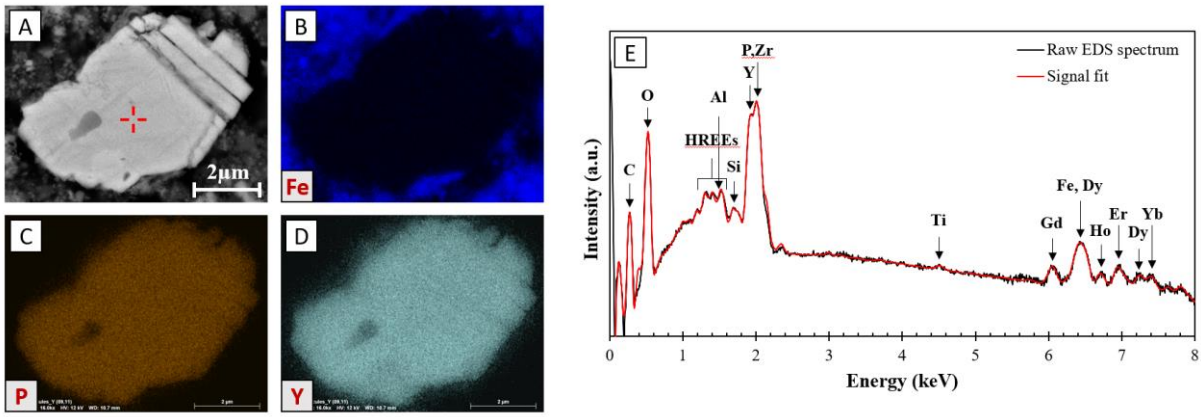

Figure 6: *(A) SEM image (BSE detector) of an yttrium particle found in samples L-BR-Gui-E as an example of lateritic bauxite residue (magnification ×4000) and associated quantitative EDS elemental maps showing the spatial distribution for (B) iron (C) phosphorus and (D) yttrium (12 kV, 50 kcps, 20 min). (E) EDS spectrum associated to the micro-analyse performed with the incident beam centered at the red cross position on (A) (15 kV, 100 kcps, 1 min).*

Scanning electron microscopy (SEM) observations coupled with energy dispersive X-ray spectroscopy (EDS) were performed on L-BR-Gui-E and K-BR-Mar-A BRs, as these two samples were assumed to be representative of lateritic and karstic BRs, respectively (***Figure 6*** and ***Figure S3***). In order to identify the occurrence of these particles in the samples in a representative way, a series of elemental distribution maps (magnification ×500) were performed on large regions of interest (6-8 mm^2) for both samples. The analytical conditions chosen allowed the identification of particles with a diameter as small as 500 nm.

In both cases, Y-rich particles were found, co-localized with similar elements. Yttrium was found co-localized with other HREEs (Gd, Dy, Ho, Er, Yb), which supports the classification of Y as HREEs and validates using it as a proxy for HREEs (Borst et al., 2020; Lallemand et al., 2022; Pingitore et al., 2014). EDS elemental maps show that Y and HREEs are always associated with phosphorus (P), but not associated with major elements (Fe, Al, Ti, Ca < 3 at%) (***Figure 6*** B, C and D). Moreover, the local chemical micro-analyses show P/HREEs atomic ratios close to 1 and Y/O atomic ratios between 0.15 and 0.25, suggesting the presence of xenotime (YPO_4) or churchite ($YPO_4.2H_2O$) phases. In rare cases, Si and Zr can also be associated (>3 at%), suggesting traces of zircon ($ZrSiO_4$) associated with xenotime, as well as with Fe from the surrounding matrix. These results are in good agreement with microscopic observations reported in the literature on BRs and bauxites (Lallemand et al., 2022; Z. Li et al., 2013; Mordberg et al., 2001; Radusinović & Papadopoulos, 2021; Reinhardt et al., 2018; Rivera et al., 2019; Vind et al., 2018). All these studies show that Y is found as xenotime or churchite phosphate particles

in BRs, as in bauxites, regardless of the origin of their geological ore, although Y has also been detected in mixed phases of REEs in Greek BRs (Vind et al., 2018).

Based on this local probe technique, it seems that Y speciation does not differ as a function of the lateritic or karstic origin of the samples and cannot confirm our hypothesis that there is a difference in HREE mineralogy between lateritic and karstic BRs based on REE patterns. However, scanning large sample areas (6-8 mm^2) indicated approximately twice as many particles present in the L-BR-Gui-E sample than in the K-BR-Mar-A sample (2.4 and 1.3 particles/mm^2 respectively) while the Y content was twice lower in the L-BR-Gui-E sample than in the K-Mar-A sample (102 and 226 mg/kg respectively). Additionally, while in both samples, most of the particle diameters were smaller than 5 µm, several large particles were found in L-BR-Gui-E, including one particle with a 50 µm diameter (***Table S5*** and ***Table S6***). This suggests that most of the Y in the K-BR-Mar-A sample is not detectable by SEM and, according to the P vs HREE scatterplot (***Figure S2***), is probably not associated with P. X-ray absorption spectroscopy (XAS) was performed at bulk scale to specifically characterise the atomic environment of Y species in all the samples, including the phosphate phases and other potential Y-bearing phases not detected by SEM analysis (Y-minerals and absorbed species).

3.5.2. X-Ray absorption spectroscopy measurements at Y K-edge

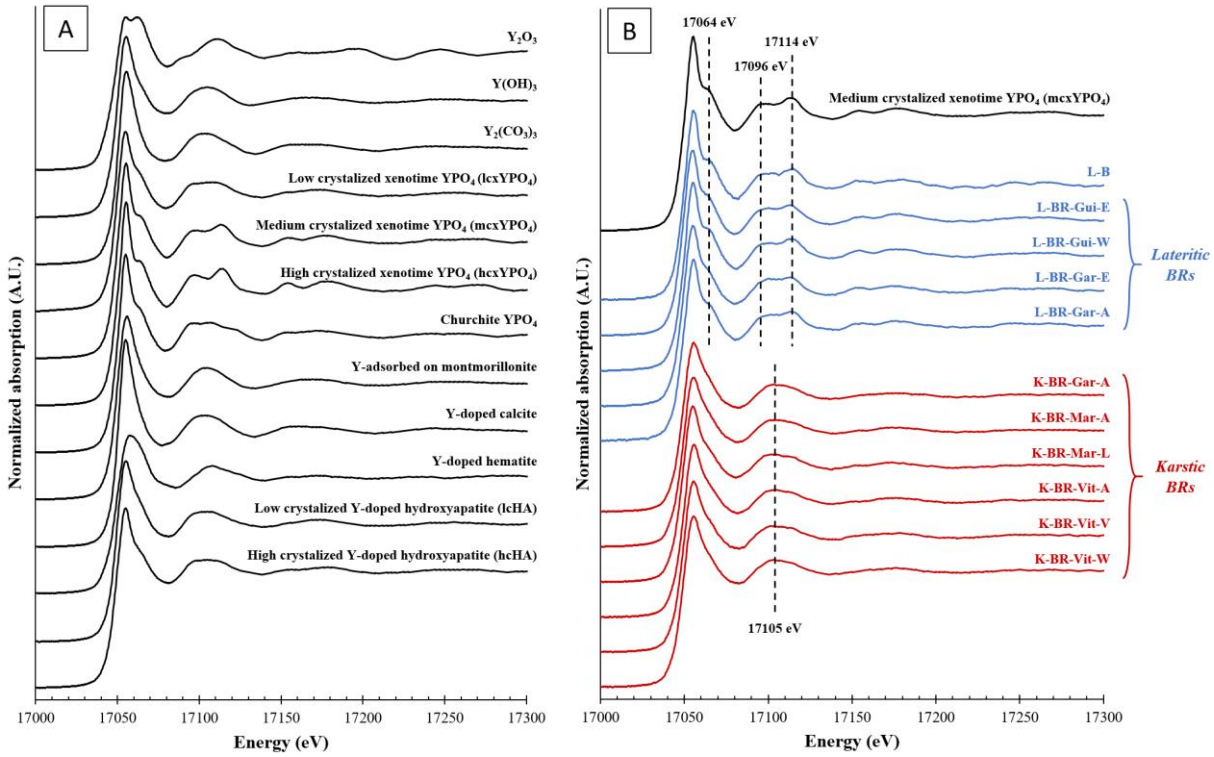

Figure 7: *(A) Stacking of Y K-edge XANES spectra of the model yttrium compounds used in the study. (B) Stacking of Y K-edge XANES spectra of all the studied samples sorted by origin of the ore (blue = lateritic-type, red = karstic-type). Spectra of crystallized YPO_4 xenotime model compound is plotted for the purpose of comparison. The main features of the spectra are identified by the dashed lines.*

The X-ray Absorption Near Edge Structure (XANES) spectra of the model compounds are shown in ***Figure 7*** A. Among them, the xenotime YPO_4 compounds show a clearly identifiable structure consisting of a shoulder after the white line at 17064 eV and a double feature at 17096 eV and 17114 eV that is repeated at 17153 and 17178 eV, these structures being more pronounced with higher crystallization. The churchite YPO_4 spectrum shows a slightly different structure with three features instead of two between 17090 and 17130 eV, allowing the xenotime to be differentiated from churchite using XAS measurements. The spectra of Y-doped hematite and Y_2O_3 are also very specific and easily identifiable. Conversely, high-crystalized Y-doped hydroxyapatite (hcHA), which is a calcium phosphate, shows very similar characteristics to those of low crystalized xenotime YPO_4 (lcxYPO_4). None of the other model compound spectra show a very specific signature but consist in a single oscillation centered around 17105 eV and little or no post-white line shoulder, making identification of the presence of these phases potentially difficult.

The Y speciation in the samples studied here can be categorised in two types of signals mainly correlated with the origin of the bauxite ore (***Figure 7*** B).

Visually, the speciation of Y in samples of lateritic origin is very similar to a xenotime phase. Indeed, linear combination fitting (LCF) of the results of the XANES region (17000 to 17220 eV) confirmed these observations with the strong presence (>34% in all best fits) of medium crystalized xenotime YPO_4 (mcxYPO_4) (***Table S7***). For example, the best fit for L-BR-Gui-E consisted in a mixture comprising 57% medium crystalized xenotime YPO_4 (mcxYPO_4) and 35% hcHA with a very good match ($\chi^2 = 0.02$) (***Figure 8*** A).

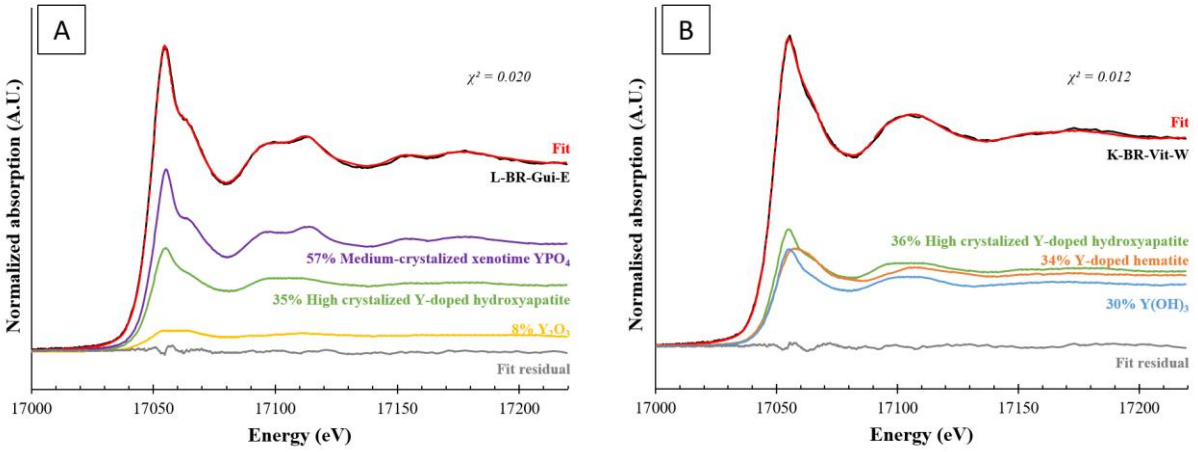

Figure 8: *Best linear combination fitting (LCF) XANES analysis results for (A) L-BR-Gui-E, as an example of lateritic samples and (B) K-BR-Vit-W, as an example of karstic samples. Fits were performed with Larch software (17000-17220 eV, with a maximum of 3 components).*

Figure 9 is a statistical study of the LCF results to compare samples with different noise levels and to obtain statistically relevant results. In ***Figure 9*** A, the percentages of occurrence of the main model compounds (with an arbitrary threshold of 25% in the fit) in all the good fits (i.e., all fits that do not statistically differ from the best fit) are plotted for each sample. A quality criterion (***Figure 9*** C), based on reduced chi-square value (χ^2_{red}), was used to determine the number of significantly good fits for each sample (***Figure 9*** B) (see section 2.2.5). Indeed, in the case of a noisy spectrum, a large number of combinations of model compounds can correctly fit the experimental data, as is the case of L-B sample with 11 fits (fit n°1 to fit n°11 in the white area) considered to be good. Thus, it does not seem reasonable to rely only on the best fit.

Our statistical study confirmed that xenotime YPO_4 appears in 100% of good fits of all lateritic samples in the form of mcxYPO_4 or less often in the form of hcxYPO_4. With the exception of the strong presence of hcHA in L-BR-Gar-A good fits, as well as $Y(OH)_3$, which was present in the majority of L-BR-Gar-E good fits, no other model compounds appear significantly in the good fits of lateritic samples. These results confirm and complement the results of the study by (Lallemand et al., 2022) who proposed

speciation of Y as a mixed amorphous and crystalline xenotime phosphate based on the same lateritic material (L-BR-Gar-E).

The speciation of Y in samples of karstic origin clearly differs from speciation in samples of lateritic origin, but is also more difficult to identify than in lateritic ones. Visually, the XANES signals do not reveal a specific structure or if they do, only tenuously. The LCF results of the XANES region showed no clear predominance (***Table S7***), as illustrated by the best fit for K-BR-Vit-W, consisting, with a very good match ($\chi^2 = 0.01$) of a mixture of 36% highly crystallized hydroxyapatite (hcHA), 34% Y-doped hematite and 30% $Y(OH)_3$ (***Figure 8*** B). Our statistical study nevertheless showed that only hcHA, Y-doped hematite, $Y(OH)_3$ and to a lesser extent, Y-adsorbed on montmorillonite, are present in the good fits of karstic BRs (***Figure 9*** A). In none of the cases, do the xenotime YPO_4 compounds stand out, in contrast to in the samples of lateritic origin. To be consistent with XAS responses, Y in karstic BRs could be adsorbed or incorporated into one or more mineral phases, as is the case for Sc in BRs (Gentzmann et al., 2021). However, Sc speciation is known to diverge from that of other REEs (Horovitz, 1975; Suss et al., 2018; Vind et al., 2018), so extrapolation to Y behaviour is not feasible. For example, in their study, Gentzmann et al. show that the geological origin of the ore implies only minor changes in the distribution of Sc in the host mineral phases, which is not the case for Y (Gentzmann et al., 2021).

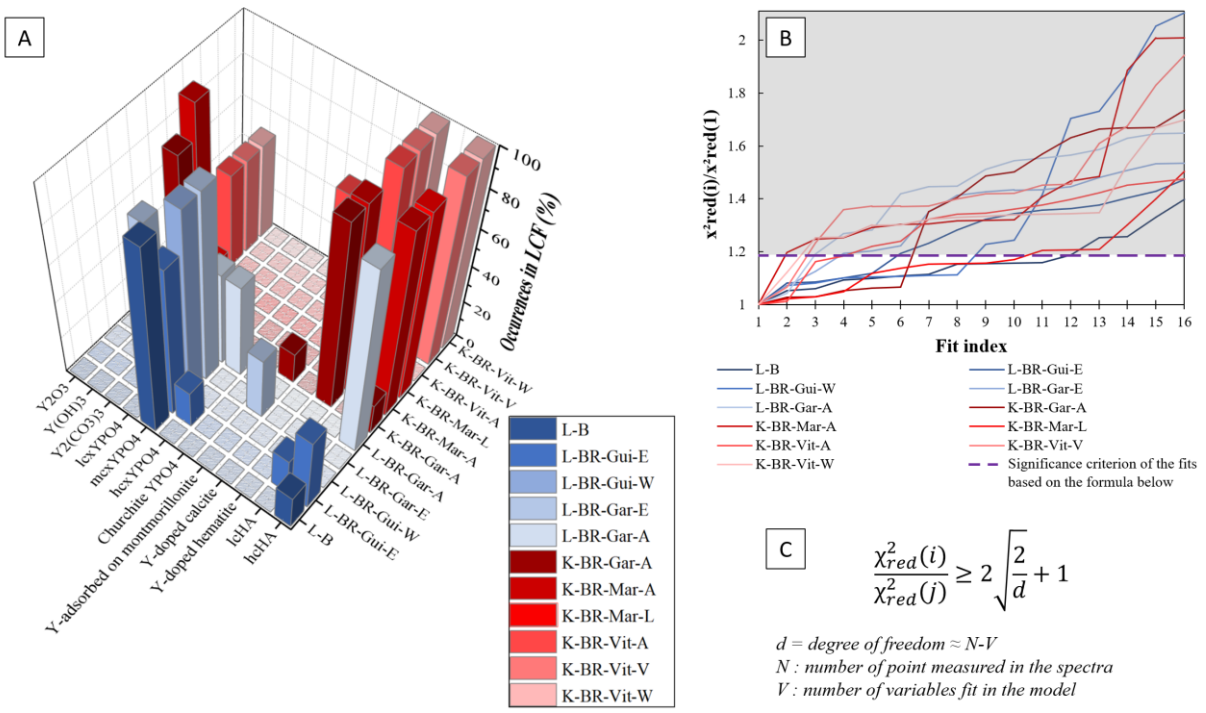

Figure 9: *(A) Occurrence of model compounds in all good fits (i.e. significantly identical to the best LCF) performed with Larch software in the XANES region (17000-17220 eV, maximum of 3 components), for all the samples studied. Only model compounds that contributed more than 25% are shown. (B) Changes in the goodness of fit (reduced-chi-square value)*

normalized by the best fit for each sample and significance cut-off criterion. Fits present in the grey area differ significantly from the best fit. (C) Significant criterion formula between two fits, i and j according to the reference (Kelly et al., 2008).

Yttrium speciation in the BRs probed by bulk XANES analysis is mainly influenced by the origin of the bauxite ore and tend to corroborate the differences between the lateritic and karstic BRs suggested by the REE patterns, contrary to the microscopic approach. In all samples of lateritic origin, Y was mainly found in the form of xenotime YPO_4, which could be distinguished from churchite YPO_4, confirming the microscopic observations. Given that YPO_4 xenotime particles were also found in karstic BRs using microscopic observation methods, but that the XANES signal indicates that the majority of Y is not in xenotime or churchite phosphate form, we can assume that Y is present in several phases in the karstic BRs. Pellet heterogeneity was also investigated by examining each XANES spectrum collected at different locations in the sample pellet before averaging, confirming the presence of rare YPO_4 particles in karstic BRs (2 out of 27 scans collected) resulting in noisier, more intense spectra and exhibiting the xenotime YPO_4 features (***Figure S4***). However, the majority of Y in karstic BRs is probably incorporated in small quantities in other mineral phases (iron oxyhydroxide, hydroxyapatite) or adsorbed on the surface of other minerals, which would explain why they are not easily detectable by SEM-EDS (below the limit of detection).

However, no variability in Y speciation was detected linked to the storage conditions of the tailings, nor their aging time for a given origin.

4. Perspectives

The information obtained in this study is crucial for the use of BRs as a secondary source of REEs, particularly for the design and implementation of selective recovery processes.

First, HREE solubility probably differs as a function of origin. Indeed, the observed difference in speciation may affect HREE recovery yields depending on the origin of the bauxite ore. A comparative study of the dissolution behaviour of HREEs from these different BRs is needed to validate this hypothesis. The solubility of HREEs was found to be very low for lateritic BRs (Lallemand et al., 2022) because of the very low solubility of xenotime. Given the higher REE content in karstic BRs than in lateritic BRs and the difference in HREE speciation, it would be interesting to test and compare similar recovery approaches. Second, the marked variability of BR storage conditions and durations does not appear to have a significant effect on HREE speciation which should consequently facilitate the treatment of tailings stored in different conditions and for different storage times at large scales.

Although origin appears to be the only parameter that affects HREE speciation, we recall that some geographical disparities may also exist due to variations in the bedrock lithology of a given origin (lateritic or karstic). In our case, bauxites ore from all lateritic BR samples came from the Boké region in Guinea (West Africa) and bauxite ore from all the karstic BR samples came from the region of Provence (South of France). Therefore, to extrapolate these results worldwide, it is crucial to study potential geological differences, including HREE speciation, for a given origin in other geographical regions of the world, such as China, Australia, Brazil or India, which are the main generators of BRs at the present time. In addition, some alumina production sites use a mixture of lateritic and karstic bauxites as ore input, e.g., at the Aluminium of Greece plant (Vind et al., 2018). In these cases, it would be impossible to address the link between the origin of the ore and HREE speciation in the BRs.

Finally, a complete understanding of REE speciation in BR remains to be achieved for LREEs, for which no clear speciation has been assigned to date.

5. Conclusion

The aim of this study was to perform a multi-scale characterisation of different bauxite residues (BRs) as a function of origin of the ore, of the storage conditions and storage time, with a particular focus on the speciation of Y as a proxy of the behaviour of heavy rare earth elements (HREEs).

We have shown that some physico-chemical properties of BRs, such as pH, conductivity or chemical composition of major elements, vary with the storage conditions and storage time and may partially explain the marked variability of physico-chemical properties of BRs reported in the literature.

More interestingly, this study has shown that other properties of the BRs, such as the mineralogy of the major phases as well as the chemical composition and speciation of the HREEs varied with the origin of the bauxite ore but were not influenced by the storage conditions or by the age of the BRs. Notably, and to our knowledge, for the first time, we were able to link the origin of the bauxite ore, lateritic or karstic, and the speciation of Y. In the case of lateritic BRs, HREEs are mostly present in the form of pure and crystallized phosphate particles (xenotime). In karstic BRs, HREEs are mainly present in a more complex speciation, probably adsorbed or incorporated in other minerals, including iron oxyhydroxide and hydroxyapatite minerals, although some xenotime phosphate particles were also detected (< 25%). Only the complementarity use of macroscopic, microscopic and spectroscopic approaches enabled us to reach a full understanding of Y speciation in these complex residues.

The present study thus paves the way for a study of the potential of BRs for the selective recovery of HREEs in a circular economy context. Our results also underline the importance of considering BRs produced in different parts of the world not as a single material but as incorporating certain disparities as a function of the origin of the ore that may require a range of different extraction processes. It is true for REEs but also for other critical elements including vanadium for example for which such eventual disparities are not documented today.

Declaration of Competing Interest

The authors declare that they have no known competing financial interests or personal relationships that could have appeared to influence the work reported in this paper.

Data Availability

Data will be made available on request.

Acknowledgments

The authors acknowledge financial support from the CNRS through the MITI interdisciplinary programmes (PRIME 2020:ExtraMet project), the *Agence Nationale de la Recherche* through the RECALL project (ANR-20-CE04-0007). The thesis contract of Claire Lallemand was funded by CEPAC (*Caisse d'épargne Provence Alpes Corse*) through the AMIDEX foundation (Aix-Marseille University). We acknowledge the European Synchrotron Radiation Facility for provision of synchrotron radiation facilities on beamline BM30. Hamed Pourkhorsandi thanks F.R.S.-FNRS for funding. The authors also thank the ACE Partner project that funded the work of Pierre Tamba Oulare (World Bank, the Association of African Universities, the French Development Agency, the Institute of Research for Development and INRIA)

Supporting information

Supplementary data associated with this article can be found in the online version at doi:10.1016/j.jhazmat.2023.132941.

References

Adewuyi, S. O., Ahmed, H. A. M., & Ahmed, H. M. A. (2020). Methods of Ore Pretreatment for Comminution Energy Reduction. *Minerals 2020, Vol. 10, Page 423*, *10*(5), 423. https://doi.org/10.3390/MIN10050423

Arnaud, C., & Guillon, J.-M. (1989). *Les Gueules Rouges. Un siècle de bauxite dans le Var*. 1st edition CDDP du Var, 1989 and augmented reedition by Association des Gueules rouges du Var, Tourves, 2003.

Baioumy, H. (2016). Factors controlling the geochemical variations of lateritic bauxites formed upon different parent rocks in Peninsular Malaysia. *Arabian Journal of Geosciences*, *9*(6), 1–15. https://doi.org/10.1007/S12517-016-2476-9/METRICS

Balaram, V. (2019). Rare earth elements: A review of applications, occurrence, exploration, analysis, recycling, and environmental impact. *Geoscience Frontiers*, *10*(4), 1285–1303. https://doi.org/10.1016/j.gsf.2018.12.005

Bardossy, G. (1982). *Karst Bauxites: Bauxite Deposits on Carbonate Rocks* (Elsevier Science Ltd (ed.); Vol. 14).

Bea, F. (1996). Residence of REE, Y, Th and U in granites and crustal protoliths; implications for the chemistry of crustal melts. *Journal of Petrology*, *37*(3). https://doi.org/10.1093/petrology/37.3.521

Belfqueh, S., Seron, A., Chapron, S., Arrachart, G., & Menad, N. (2022). Evaluating organic acids as alternative leaching reagents for rare earth elements recovery from NdFeB magnets. *Journal of Rare Earths*. https://doi.org/10.1016/J.JRE.2022.04.027

Bhukte, P. G., Daware, G. T., Masurkar, S. P., Mahendiran, P., Janbandhu, K., Rao, K. R., Singh, U., Puttewar, S. P., & Agnihotri, A. (2020). Geochemical, Mineralogical and Petrological Characteristics of Lateritic Bauxite Deposits formed on Deccan Trap Basalt with Reference to High-level and Coastal (low level) Deposits of Maharashtra. *Journal of the Geological Society of India*, *95*(6), 587–598. https://doi.org/10.1007/S12594-020-1485-1/METRICS

Binnemans, K., Jones, P. T., Blanpain, B., Van Gerven, T., & Pontikes, Y. (2015). Towards zero-waste valorisation of rare-earth-containing industrial process residues: A critical review. *Journal of Cleaner Production*, *99*, 17–38. https://doi.org/10.1016/j.jclepro.2015.02.089

Borra, C. R., Blanpain, B., Pontikes, Y., Binnemans, K., & Van Gerven, T. (2016). Recovery of Rare Earths and Other Valuable Metals From Bauxite Residue (Red Mud): A Review. *Journal of Sustainable Metallurgy*, *2*(4), 365–386. https://doi.org/10.1007/s40831-016-0068-2

Borst, A. M., Smith, M. P., Finch, A. A., Estrade, G., Villanova-de-Benavent, C., Nason, P., Marquis, E., Horsburgh, N. J., Goodenough, K. M., Xu, C., Kynický, J., & Geraki, K. (2020). Adsorption of rare earth elements in regolith-hosted clay deposits. *Nature Communications*, *11*(1), 1–15. https://doi.org/10.1038/s41467-020-17801-5

British Geological Survey. (2015). *Risk list 2015: an update to the supply risk indexfor elements or element groups that are of economic value.* https://www2.bgs.ac.uk/mineralsuk/statistics/risklist.html

Chaurand, P., Collin, B., Couturier, J., Lallemand, C., & Levard, C. (2025). *Insights into Yttrium speciation in bauxite residue before and after unconventional leaching experiments [Data set]*. https://doi.org/doi.org/10.15151/ESRF-ES-806199268

Chen, Y., & Zheng, B. (2019). *sustainability What Happens after the Rare Earth Crisis: A Systematic Literature Review*. https://doi.org/10.3390/su11051288

Couturier, J., Lallemand, C., Levard, C., Chaurrand, P., Rose, J., & Collin, B. (2022). Y K edge XAS transmission and XAS fluorescence of Yttrium components at 20K. [Dataset/Spectral Data]. *SSHADE/FAME (OSUG Data Center)*. https://doi.org/10.26302/SSHADE/EXPERIMENT_JC_20220615_001

Cusack, P. B., Courtney, R., Healy, M. G., O' Donoghue, L. M. T., & Ujaczki, É. (2019). An evaluation of the general composition and critical raw material content of bauxite residue in a storage area over a twelve-year period. *Journal of Cleaner Production*, *208*, 393–401. https://doi.org/10.1016/j.jclepro.2018.10.083

Davris, P., Balomenos, E., Taxiarchou, M., Panias, D., & Paspaliaris, I. (2017). Current and Alternative Routes in the Production of Rare Earth ElementsAktuelle und alternative Routen bei der Herstellung von Metallen der Seltenen Erden. *BHM Berg- Und Hüttenmännische Monatshefte*, *162*(7), 245–251. https://doi.org/10.1007/s00501-017-0610-y

De Oliveira, S. B., Da Costa, M. L., & Dos Prazeres Filho, H. J. (2016). THE LATERITIC BAUXITE DEPOSIT OF RONDON DO PARÁ: A NEW GIANT DEPOSIT IN THE AMAZON REGION, NORTHERN BRAZIL. *Economic Geology*, *111*(5), 1277–1290. https://doi.org/10.2113/ECONGEO.111.5.1277

Deady, É., Mouchos, E., Goodenough, K., Williamson, B., & Wall, F. (2014). Rare Earth Elements in Karst-Bauxites: a Novel Untapped European Resource? *ERES 2014 : 1st Conference on European Rare Earth Resources, Milos, Greece. (Unpublished)* , 364–375. https://nora.nerc.ac.uk/id/eprint/508643/

Di Carlo, E., Chen, C. R., Haynes, R. J., Phillips, I. R., & Courtney, R. (2019). Soil quality and vegetation performance indicators for sustainable rehabilitation of bauxite residue disposal areas: A review. In *Soil Research* (Vol. 57, Issue 5, pp. 419–446). CSIRO. https://doi.org/10.1071/SR18348

Dupont, D., & Binnemans, K. (2015). Recycling of rare earths from NdFeB magnets using a combined leaching/extraction system based on the acidity and thermomorphism of the ionic liquid [Hbet][Tf2N]. *Green Chemistry*, *17*(4), 2150–2163. https://doi.org/10.1039/c5gc00155b

Eheliyagoda, D., Zeng, X., & Li, J. (2020). A method to assess national metal criticality: the environment as a foremost measurement. *Humanities and Social Sciences Communications 2020*

7:1, *7*(1), 1–12. https://doi.org/10.1057/s41599-020-00537-4

European Commission. (2020). *Critical Raw Materials for Strategic Technologies and Sectors in the EU. A Foresight Study*. https://doi.org/10.2873/865242

Evans, K. (2016). The History, Challenges, and New Developments in the Management and Use of Bauxite Residue. *Journal of Sustainable Metallurgy*, *2*(4), 316–331. https://doi.org/10.1007/S40831-016-0060-X/FIGURES/14

Farjana, S. H., Huda, N., Parvez Mahmud, M. A., & Saidur, R. (2019). A review on the impact of mining and mineral processing industries through life cycle assessment. *Journal of Cleaner Production*, *231*, 1200–1217. https://doi.org/10.1016/j.jclepro.2019.05.264

Fourrier, C. (2020). *Les résidus de bauxite de Provence : propriétés physico-chimiques et influence sur la formation et le fonctionnement des sols [Thesis]*. Aix-Marseille university (ED 251).

Fourrier, C., Luglia, M., Keller, C., Hennebert, P., Foulon, J., Ambrosi, J. P., Angeletti, B., & Criquet, S. (2021). How Raw and Gypsum Modified Bauxite Residues Affect Seed Germination, Enzyme Activities, and Root Development of Sinapis alba. *Water, Air, and Soil Pollution*, *232*(8). https://doi.org/10.1007/s11270-021-05232-x

Freyssinet, P., Butt, C. R. M., Morris, R. C., & Piantone, P. (2005). Ore-Forming Processes Related to Lateritic Weathering. In *One Hundredth Anniversary Volume*. Society of Economic Geologists. https://doi.org/10.5382/AV100.21

Gauß Roland, Burkhardt Carlo, Carencotte Frédéric, Gasparon Massimo, Gutfleisch Oliver, Higgins Ian, Karajić Milana, Klossek Andreas, Mäkinen Maija, Schäfer Bernd, Reinhold Schindler, & Badrinath Veluri. (2021). *Rare Earth Magnets and Motors: A European Call for Action. A report by the Rare Earth Magnets and Motors Cluster of the European Raw Materials Alliance*.

Gentzmann, M. C., Schraut, K., Vogel, C., Gäbler, H. E., Huthwelker, T., & Adam, C. (2021). Investigation of scandium in bauxite residues of different origin. *Applied Geochemistry*, *126*. https://doi.org/10.1016/j.apgeochem.2021.104898

Goodland, R. (2012). Responsible mining: The key to profitable resource development. *Sustainability*, *4*(9), 2099–2126. https://doi.org/10.3390/SU4092099

Gräfe, M., Power, G., & Klauber, C. (2011). Bauxite residue issues: III. Alkalinity and associated chemistry. *Hydrometallurgy*, *108*(1–2). https://doi.org/10.1016/j.hydromet.2011.02.004

Grohol, M., & Veeh, C. (2023). *Study on the Critical Raw Materials for the EU 2023 Final Report*. https://doi.org/10.2873/725585

Gschneidner, K. A. (1990). Physical properties of the rare earth metals. *Bulletin of Alloy Phase Diagrams*, *11*(3), 216–224. https://doi.org/10.1007/BF03029283

Gu, J., Huang, Z., Fan, H., Jin, Z., Yan, Z., & Zhang, J. (2013). *Mineralogy, geochemistry, and genesis of lateritic bauxite deposits in the Wuchuan-Zheng'an-Daozhen area, Northern Guizhou Province, China*. https://doi.org/10.1016/j.gexplo.2013.03.003

Hatayama, H., & Tahara, K. (2014). *Criticality Assessment of Metals for Japan's Resource Strategy*.

https://doi.org/10.2320/matertrans.M2014380
Haynes, W. M. (2014). Section 14 - Geophysics, Astronomy, and Acoustics. In *CRC Handbook of Chemistry and Physics*. https://doi.org/10.1201/b17118-19
Hermassi, M., Granados, M., Valderrama, C., Ayora, C., & Cortina, J. L. (2022). Recovery of rare earth elements from acidic mine waters: An unknown secondary resource. *Science of the Total Environment*, *810*. https://doi.org/10.1016/j.scitotenv.2021.152258
Horovitz, C. T. (1975). *Scandium : its occurrence, chemistry, physics, metallurgy, biology, and technology*. Academic Press. https://doi.org/10.1016/B978-0-12- 355850-3.X5001-1
Huang, Y., He, H., Liang, X., Bao, Z., Tan, W., Ma, L., Zhu, J., Huang, J., & Wang, H. (2021). Characteristics and genesis of ion adsorption type REE deposits in the weathering crusts of metamorphic rocks in Ningdu, Ganzhou, China. *Ore Geology Reviews*, *135*, 104173. https://doi.org/10.1016/J.OREGEOREV.2021.104173
International Aluminium Institute. (2023, January 26). *Alumina Production*. https://international-aluminium.org/statistics/alumina-production/
International Energy Agency. (2021). *The Role of Critical World Energy Outlook Special Report Minerals in Clean Energy Transitions*. https://www.iea.org/reports/the-role-of-critical-minerals-in-clean-energy-transitions
Jones, B. E. H., Haynes, R. J., & Phillips, I. R. (2012). Cation and anion leaching and growth of Acacia saligna in bauxite residue sand amended with residue mud, poultry manure and phosphogypsum. *Environmental Science and Pollution Research*, *19*(3). https://doi.org/10.1007/s11356-011-0630-1
Kelly, S. D., Hesterberg, D., & Ravel, B. (2008). Analysis of Soils and Minerals Using X-ray Absorption Spectroscopy. *Methods of Soil Analysis, Part 5: Mineralogical Methods*, *5*, 387–463. https://doi.org/10.2136/SSSABOOKSER5.5.C14
Khairul, M. A., Zanganeh, J., & Moghtaderi, B. (2019). The composition, recycling and utilisation of Bayer red mud. *Resources, Conservation and Recycling*, *141*, 483–498. https://doi.org/10.1016/j.resconrec.2018.11.006
Khaitan, S., Dzombak, D. A., & Lowry, G. V. (2009). Neutralization of Bauxite Residue with Acidic Fly Ash. *Environmental Engineering Science*, *26*(2). https://doi.org/10.1089/ees.2007.0232
Khaitan, S., Dzombak, D. A., Swallow, P., Schmidt, K., Fu, J., & Lowry, G. V. (2010). Field Evaluation of Bauxite Residue Neutralization by Carbon Dioxide, Vegetation, and Organic Amendments. *Journal of Environmental Engineering*, *136*(10). https://doi.org/10.1061/(asce)ee.1943-7870.0000230
Klauber, C., Gräfe, M., & Power, G. (2011). Bauxite residue issues: II. options for residue utilization. *Hydrometallurgy*, *108*(1–2). https://doi.org/10.1016/j.hydromet.2011.02.007
Kloprogge, J. T., Ruan, H. D., & Frost, R. L. (2002). Thermal decomposition of bauxite minerals: Infrared emission spectroscopy of gibbsite, boehmite and diaspore. *Journal of Materials Science*,

37(6), 1121–1129. https://doi.org/10.1023/A:1014303119055/METRICS

Kong, X., Guo, Y., Xue, S., Hartley, W., Wu, C., Ye, Y., & Cheng, Q. (2017). Natural evolution of alkaline characteristics in bauxite residue. *Journal of Cleaner Production*, *143*, 224–230. https://doi.org/10.1016/J.JCLEPRO.2016.12.125

Kong, X., Li, M., Xue, S., Hartley, W., Chen, C., Wu, C., Li, X., & Li, Y. (2017). Acid transformation of bauxite residue: Conversion of its alkaline characteristics. *Journal of Hazardous Materials*, *324*(Pt B), 382–390. https://doi.org/10.1016/J.JHAZMAT.2016.10.073

Lallemand, C., Ambrosi, J. P., Borschneck, D., Angeletti, B., Chaurand, P., Campos, A., Desmau, M., Fehlauer, T., Auffan, M., Labille, J., Roche, N., Poizat, L., Collin, B., Rose, J., & Levard, C. (2022). Potential of Ligand-Promoted Dissolution at Mild pH for the Selective Recovery of Rare Earth Elements in Bauxite Residues. *ACS Sustainable Chemistry & Engineering*, *10*(21), 6942–6951. https://doi.org/10.1021/acssuschemeng.1c08081

Li, M. Y. H., Zhou, M. F., & Williams-Jones, A. E. (2019). The Genesis of Regolith-Hosted Heavy Rare Earth Element Deposits: Insights from the World-Class Zudong Deposit in Jiangxi Province, South China. *Economic Geology*, *114*(3), 541–568. https://doi.org/10.5382/ECONGEO.4642

Li, Z., Din, J., Xu, J., Liao, C., Yin, F., Lü, T., Cheng, L., & Li, J. (2013). *Discovery of the REE minerals in the Wulong-Nanchuan bauxite deposits, Chongqing, China: Insights on conditions of formation and processes*. https://doi.org/10.1016/j.gexplo.2013.06.016

Liu, X., Wang, Q., Zhang, Q., Zhang, Y., & Li, Y. (2016). Genesis of REE minerals in the karstic bauxite in western Guangxi, China, and its constraints on the deposit formation conditions. *Ore Geology Reviews*, *75*, 100–115. https://doi.org/10.1016/J.OREGEOREV.2015.12.015

Ma, Y., Preveniou, A., Kladis, A., & Pettersen, J. B. (2022). Circular economy and life cycle assessment of alumina production: Simulation-based comparison of Pedersen and Bayer processes. *Journal of Cleaner Production*, *366*. https://doi.org/10.1016/J.JCLEPRO.2022.132807

Macías-Pérez, L. A., Levard, C., Barakat, M., Angeletti, B., Borschneck, D., Poizat, L., Achouak, W., & Auffan, M. (2022). Contrasted microbial community colonization of a bauxite residue deposit marked by a complex geochemical context. *Journal of Hazardous Materials*, *424*. https://doi.org/10.1016/j.jhazmat.2021.127470

Menzies, N. W., & Kopittke, P. M. (2021). Seawater neutralization and gypsum amelioration of bauxite refining residue to produce a plant growth medium. *Science of the Total Environment*, *763*. https://doi.org/10.1016/j.scitotenv.2020.143046

Michalowicz, A., Moscovici, J., Muller Bouvet, D., & Provost, K. (2009). MAX: Multiplatform Applications for XAFS. *Journal of Physics: Conference Series*, *190*(1), 012034. https://doi.org/10.1088/1742-6596/190/1/012034

Mondillo, N., Balassone, G., Boni, M., Chelle-Michou, C., Cretella, S., Mormone, A., Putzolu, F., Santoro, L., Scognamiglio, G., & Tarallo, M. (2019). Rare Earth Elements (REE) in Al- and Fe-

(Oxy)-Hydroxides in Bauxites of Provence and Languedoc (Southern France): Implications for the Potential Recovery of REEs as By-Products of Bauxite Mining. *Minerals 2019, Vol. 9, Page 504*, *9*(9), 504. https://doi.org/10.3390/MIN9090504

Mordberg, L. E., Stanley, C. J., & Germann, K. (2001). Mineralogy and geochemistry of trace elements in bauxites: the Devonian Schugorsk deposit, Russia. *Mineralogical Magazine*, *65*(1). https://doi.org/10.1180/002646101550145

Negrão, L. B. A., & Costa, M. L. da. (2021). Mineralogy and geochemistry of a bauxite-bearing lateritic profile supporting the identification of its parent rocks in the domain of the huge Carajás iron deposits, Brazil. *Journal of South American Earth Sciences*, *108*, 103164. https://doi.org/10.1016/J.JSAMES.2021.103164

Newville, M. (2013). Larch: An Analysis Package for XAFS and Related Spectroscopies. *Journal of Physics: Conference Series*, *430*(1), 012007. https://doi.org/10.1088/1742-6596/430/1/012007

Ochsenkiihn-Petropulu, M., Lyberopulu, T., Ochsenkiihn ', K. M., & Parissakis, G. (1996). Recovery of lanthanides and yttrium from red mud leaching by selective. *Analytica Chimica Acta*, *319*, 249–254.

OECD. (2019). *Global Material Resources Outlook to 2060 Economic drivers and environmental consequences*.

Peiravi, M., Dehghani, F., Ackah, L., Baharlouei, A., Godbold, J., Liu, J., Mohanty, M., & Ghosh, T. (2021). A Review of Rare-Earth Elements Extraction with Emphasis on Non-conventional Sources: Coal and Coal Byproducts, Iron Ore Tailings, Apatite, and Phosphate Byproducts. In *Mining, Metallurgy and Exploration* (Vol. 38, Issue 1). https://doi.org/10.1007/s42461-020-00307-5

Pingitore, N., Clague, J., & Gorski, D. (2014). Round Top Mountain rhyolite (Texas, USA), a massive, unique Y-bearing-fluorite-hosted heavy rare earth element (HREE) deposit. *JOURNAL OF RARE EARTHS*, *32*(1). https://doi.org/10.1016/S1002-0721(14)60037-5

Power, G., Gräfe, M., & Klauber, C. (2011). Bauxite residue issues: I. Current management, disposal and storage practices. *Hydrometallurgy*, *108*(1–2), 33–45. https://doi.org/10.1016/J.HYDROMET.2011.02.006

Prior, T., Giurco, D., Mudd, G., Mason, L., & Behrisch, J. (2012). Resource depletion, peak minerals and the implications for sustainable resource management. *Global Environmental Change*, *22*(3), 577–587. https://doi.org/10.1016/J.GLOENVCHA.2011.08.009

Qu, Y., & Lian, B. (2013). Bioleaching of rare earth and radioactive elements from red mud using Penicillium tricolor RM-10. *Bioresource Technology*, *136*, 16–23. https://doi.org/10.1016/j.biortech.2013.03.070

Radomirovic, T., Smith, P., Southam, D., Tashi, S., & Jones, F. (2013). Crystallization of sodalite particles under Bayer-type conditions. *Hydrometallurgy*, *137*, 84–91. https://doi.org/10.1016/J.HYDROMET.2013.05.006

Radusinović, S., & Papadopoulos, A. (2021). The potential for REE and associated critical metals in karstic bauxites and bauxite residue of Montenegro. *Minerals*, *11*(9). https://doi.org/10.3390/min11090975

Ramprasad, C., Gwenzi, W., Chaukura, N., Izyan, N., Azelee, W., Rajapaksha, A. U., Naushad, M., & Rangabhashiyam, S. (2022). Strategies and options for the sustainable recovery of rare earth elements from electrical and electronic waste. *Chemical Engineering Journal*, *442*, 1385–8947. https://doi.org/10.1016/j.cej.2022.135992

Rayzman, V. L. (1998). Red mud revisited - Special paper on scandium potential. *Aluminium Today*, *10*(5), 64–68. https://www.proquest.com/openview/40883cf8bf5b1dae72ffc50c5a8ec9a7/1?pq-origsite=gscholar&cbl=1056345

Reinhardt, N., Proenza, J. A., Villanova-De-benavent, C., Aiglsperger, T., Bover-Arnal, T., Torró, L., Salas, R., & Dziggel, A. (2018). Geochemistry and mineralogy of rare earth elements (REE) in bauxitic ores of the catalan coastal range, NE Spain. *Minerals*, *8*(12). https://doi.org/10.3390/min8120562

Rivera, R. M., Ounoughene, G., Malfliet, A., Vind, J., Panias, D., Vassiliadou, V., Binnemans, K., & Van Gerven, T. (2019). A Study of the Occurrence of Selected Rare-Earth Elements in Neutralized–Leached Bauxite Residue and Comparison with Untreated Bauxite Residue. *Journal of Sustainable Metallurgy 2019 5:1*, *5*(1), 57–68. https://doi.org/10.1007/S40831-018-0206-0

Santini, T. C., & Fey, M. V. (2013). Spontaneous vegetation encroachment upon bauxite residue (red mud) as an indicator and facilitator of in situ remediation processes. *Environmental Science and Technology*, *47*(21). https://doi.org/10.1021/es402924g

Scheidel, A., Del Bene, D., Liu, J., Navas, G., Mingorría, S., Demaria, F., Avila, S., Roy, B., Ertör, I., Temper, L., & Martínez-Alier, J. (2020). Environmental conflicts and defenders: A global overview. *Global Environmental Change*, *63*. https://doi.org/10.1016/J.GLOENVCHA.2020.102104

Senaputra, A., Fawell, P., Jones, F., & Smith, P. (2012). The impact of desilication product on bauxite residue flocculation. *9th Alumina Quality Workshop*, 186–192. https://espace.curtin.edu.au/bitstream/20.500.11937/39817/2/191263_191263.pdf

Sidibe, M., & Yalcin, M. G. (2018). *Petrography, mineralogy, geochemistry and genesis of the Balaya bauxite deposits in Kindia region, Maritime Guinea, West Africa*. https://doi.org/10.1016/j.jafrearsci.2018.08.017

Smith, P. (2009). The processing of high silica bauxites — Review of existing and potential processes. *Hydrometallurgy*, *98*(1–2), 162–176. https://doi.org/10.1016/J.HYDROMET.2009.04.015

Snars, K., & Gilkes, R. J. (2009). Evaluation of bauxite residues (red muds) of different origins for environmental applications. *Applied Clay Science*, *46*(1). https://doi.org/10.1016/j.clay.2009.06.014

Suss, A., Panov, A., Kozyrev, A., Kuznetsova, N., & Gorbachev, S. (2018). Specific features of

scandium behavior during sodium bicarbonate digestion of red mud. *Minerals, Metals and Materials Series*, *Part F4*, 165–173. https://doi.org/10.1007/978-3-319-72284-9_22/COVER

Taylor, S. R., & McLennan, S. M. (1985). The Continental Crust: Its Composition and Evolution. *Geological Magazine*, *122*(6), 673–674. https://doi.org/10.1017/S0016756800032167

Torró, L., Proenza, J. A., Aiglsperger, T., Bover-Arnal, T., Villanova-de-Benavent, C., Rodríguez-García, D., Ramírez, A., Rodríguez, J., Mosquea, L. A., & Salas, R. (2017). Geological, geochemical and mineralogical characteristics of REE-bearing Las Mercedes bauxite deposit, Dominican Republic. *Ore Geology Reviews*, *89*. https://doi.org/10.1016/j.oregeorev.2017.06.017

U.S. Geological Survey, D. of the interior. (2022). 2022 Final List of Critical Minerals. In *Federal Register, Vol. 87, No. 37* (pp. 10381–10382). American Association for the Advancement of Science.

Vind, J., Malfliet, A., Blanpain, B., Tsakiridis, P. E., Tkaczyk, A. H., Vassiliadou, V., & Panias, D. (2018). Rare earth element phases in bauxite residue. *Minerals*, *8*(2). https://doi.org/10.3390/min8020077

Wagh, A. S., & Pinnock, W. R. (1987). Occurrence of scandium and rare earth elements in Jamaican bauxite waste. *Economic Geology*, *82*(3), 757–761. https://doi.org/10.2113/gsecongeo.82.3.757

Wong, J. W. C., & Ho, G. E. (1991). Effects of gypsum and sewage sludge amendment on physical properties of fine bauxite refining residue. *Soil Science*, *152*(5). https://doi.org/10.1097/00010694-199111000-00003

Wu, Y., Li, M., Fu, D., Santini, T. C., Jiang, J., Hartley, W., & Xue, S. (2020). Simulation study for the formation of alkaline efflorescence on bauxite residue disposal areas following the phosphogypsum addition. *Journal of Cleaner Production*, *262*. https://doi.org/10.1016/j.jclepro.2020.121266

Xue, S., Zhu, F., Kong, X., Wu, C., Huang, L., Huang, N., & Hartley, W. (2016). A review of the characterization and revegetation of bauxite residues (Red mud). *Environmental Science and Pollution Research*, *23*(2). https://doi.org/10.1007/s11356-015-4558-8

Yang, F., Kubota, F., Baba, Y., Kamiya, N., & Goto, M. (2013). Selective extraction and recovery of rare earth metals from phosphor powders in waste fluorescent lamps using an ionic liquid system. *Journal of Hazardous Materials*, *254–255*(1), 79–88. https://doi.org/10.1016/J.JHAZMAT.2013.03.026

Zepf, V., Simmons, J., Reller, A., Ashfield, M., & Rennie, C. (2014). *Materials critical to the energy industry. An introduction. 2nd edition.*

Zhu, F., Xue, S., Hartley, W., Huang, L., Wu, C., & Li, X. (2016). Novel predictors of soil genesis following natural weathering processes of bauxite residues. *Environmental Science and Pollution Research*, *23*(3). https://doi.org/10.1007/s11356-015-5537-9